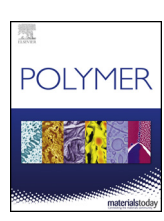


Contents lists available at ScienceDirect

Polymer

journal homepage: www.elsevier.com/locate/polymer



Growth of anisotropic single crystals of a random copolymer, poly[(R)-3-hydroxybutyrate-co-(R)-3-hydroxyhexanoate] driven by cooperative –CH···O H-bonding



Changhao Liu^a, Isao Noda^{a,b}, David C. Martin^a, D. Bruce Chase^a, Chaoying Ni^a, John F. Rabolt^{a,*}

- ^a Department of Materials Science and Engineering, University of Delaware, Newark, DE, USA
- ^b Danimer Scientific, Bainbridge, GA, USA

HIGHLIGHTS

- Single crystals of a random copolymer, PHBHx, with 3.9 mol% of 3HHx were grown.
- The 3HHx comonomer is excluded from the lattice as a non-crystallizable defect.
- \bullet All samples grown at different T_c formed well-developed needle-shaped single crystals.
- A very anisotropic lateral growth habit of the single crystals was observed.
- \bullet The growth rate along a axis was observed to be much higher than that along the b axis.

ARTICLE INFO

Keywords: Single crystals Anisotropic growth habits H-bonding

ABSTRACT

Single crystals of a random copolymer, Poly[(R)-3-hydroxybutyrate-co-(R)-3-hydroxyhexanoate] (PHBHx), with a relatively high (R)-3-hydroxyhexanoate (3HHx) content of 3.9 mol% were grown from dilute solutions over a wide range of crystallization temperatures (T_c) from $-20\,^{\circ}\text{C}$ to 75 $^{\circ}\text{C}$. Unlike Poly[(R)-3-hydroxybutyrate-co-(R)-3-hydroxyvalerate] (PHBV) which allows the 3-hydroxyvalerate (3HV) to be included into PHB lattice, 3HHx is excluded from the lattice as a non-crystallizable molecular defect. Remarkably, however, even at such a high defect content, all the samples (except for $T_c = -20$ °C) formed well-developed needle-shaped single crystals, with a crystal morphology similar to that found for crystals of the homopolymer PHB. A very characteristic anisotropic lateral growth habit is observed, with the growth rate along the a axis being much higher than that along the b axis. This anisotropic growth pattern was significantly enhanced at $T_c = 20$ °C, wherein the unit cell packing velocity along the a direction is approximately 55 times faster than that along the b direction. This thermal dependent anisotropy was attributed to an unusual cooperative hydrogen bond-like network formed by methyl hydrogen and a neighboring carbonyl oxygen in the α crystal of PHB. Another manifestation of this Hbonding network can be seen in unusually thin crystal lamellae at $-20\,^{\circ}$ C, with only ~ 6 repeat units per stem, suggesting a superior stability of crystal structure. Interestingly, at this temperature, although 3HHx still cannot be accommodated along the a direction (the H-bonding direction), it could be included along the b direction, indicated by the observation of lattice expansion along the b direction. Also at $T_c = -20$ °C, we found that 3HHx began to show some impact on the crystalline morphology, indicated by the development of a twisted lamellar texture. This effect was believed to arise from the release of stress induced by a congested fold surface dominated by non-crystalline 3HHx and 3HB units.

1. Introduction

Poly[(R)-3-hydroxybutyrate-co-(R)-3-hydroxyhexanoate] (PHBHx), a relatively new polyhydroxyalkanoate (PHA), is a bio-based, semi-crystalline, random copolymer which can be bio-synthesized through

bacterial fermentation [1–4]. It has drawn great attention due to its favorable mechanical properties, superior biodegradability and biocompatibility [5–7]. By incorporating 3HHx comonomer units, the application of PHBHx has been greatly expanded to include use as tough and ductile bioplastics and elastomers. Recently, this class of

E-mail address: rabolt@udel.edu (J.F. Rabolt).

^{*} Corresponding author.

biopolymers also has drawn attention from the field of polymer physics due to the discovery by Sato et al. [8] of the existence of a weak C-H...O hydrogen-like bond. This observation was reported as the first case of weak hydrogen bonding involving C-H groups in a semi crystalline polymer system. Later on, Wang and Tashiro refined the PHB crystal structure and determined the coordinates of hydrogen atoms in the unit cell by resolving the crystal structure of PHB thin films with short wavelength X-ray diffraction (XRD) [9]. They further confirmed that the distance, d, between the methyl hydrogen and carbonyl oxygen is indeed shorter than the sum of Van der Waals radii of the two atoms. with a value of 2.62 Å, indicative of a comparatively close interaction existing between them. The first evidence of weak H-bonding in organic crystal structures involving hydrogen atoms bonded to a sp [3] hybridized carbon was observed in the crystal structure of dimethyl oxalate [10]. It was manifested by an anomalously high melting point, 54 °C, 100 °C higher than related carboxylic acid esters [11]. Later, several other organic molecules including 1-methoxy-2-(dimethylamino)ethane were shown to possess a strong interaction between methyl hydrogen and methoxy oxygen [12]. In biological systems, the role of such a low interactive energy H-bond has been found more frequently and presumably acts cooperatively to stabilize the molecular conformation and specificity [13,14]. However, in the field of materials science, reported cases involving weak hydrogen bonding in solid state material structures are limited. To our knowledge, the class of PHB is the only documented case exhibiting weak cooperative H-bonding behavior. However, the potential impacts of these structures on crystallization behavior are still not clear.

In addition, another peculiar behavior of PHBHx can be sensed from its origin. After the initial discovery of PHB, it was quickly realized that the homopolymer had limited practical use due to a high melting point near the degradation temperature and an extremely high crystallinity (up to 90%) [15] leading to a highly brittle material. Extensive efforts have been made to decrease the overall crystallinity of PHB. Early attempts involved copolymerizing 3-hydroxyvalerate (3HV) into PHB backbone. It turned out that the crystallinity of PHBV was still remarkably high, over 60% due to isodimorphism wherein co-crystallization occurred over the entire composition of 3HV by either accommodating 3HV into the PHB lattice or vice versa [16]. Later on, 3HHx was found to be able to significantly disrupt the crystallinity. However, although the final crystallinity for the bulk PHBHx can be brought down to 30%, the required using amount of 3HHx to effectively disrupt the crystallinity is significantly higher than predicted, reaching 13 mol%, or even higher. This observation is indeed counter-intuitive because normally an incorporation of even ~1 mol% defects, such as seen for propyl-branched PE would significantly decrease the crystallinity [17]. However, the difficulty of inhibiting the crystallization of PHB through incorporating non-crystallized comonomer has not received much attention and the origins of this peculiarity has also not been clear on the molecular level till now.

We hypothesized that the surprisingly superior crystallization ability of both PHB and PHBHx are intrinsically related to this weak hydrogen bonding. In the present study, we attempted to provide supporting evidence for this hypothesis by growing single crystals of PHBHx from dilute solution, to show that these weak cooperative Hbonding sites indeed affect the crystal growth habits and stabilizes the crystal structure. To illustrate that point, PHBHx with a 3.9 mol% 3HHx comonomer concentration, normally regarded as introducing a high level of defects, was used, and single crystals were grown over a wide range of crystallization temperatures. The structure and growth habits of the crystals were studied using transmission electron microscopy, Xray diffraction, and infrared spectroscopy. A unit cell structure was constructed to illustrate the coordinated molecular packing style due to the H-bonding. The influence of the weak cooperative hydrogen bonding in lamellar thickness was also investigated. The mechanism of 3HHx influencing PHBHx crystallization was illustrated by comparing it with that of 3HV in the case of PHBV.

2. Experimental section

2.1. Materials

Poly[(R)-3-hydroxybutyrate-co-(R)-3-hydroxyhexanoate] (PHBHx), under the trade name Nodax™, with 3.9 mol% 3HHx content was supplied by the Procter & Gamble Company (Cincinnati, OH, USA). The weight average molecular weight of the polymer was 843,000 g/mol. For this class of copolymer, the random distribution nature for both of the monomer units 3HB and 3HHx has been confirmed using electrospray ionisation multistage mass spectrometry (ESI-MS¹n) reported previously [18]. As-received powder was purified by first dissolving in chloroform followed by filtration and subsequent precipitation in hexane to remove nonpolar impurities. The polymer was then re-dissolved in chloroform followed by precipitation in methanol to remove polar impurities. The as-purified polymer was then powdered and dried at room temperature under vacuum to remove residual solvent.

2.2. Preparation of PHBHx single crystals

A modified preparation method for growing single crystals of PHBHx was used [19]. A phase diagram of temperature versus solvent ratio (chloroform/ethanol) was plotted using preliminary data (see supporting information part 1 1.1). Special care was given to ensure strict isothermal crystallization (see supporting information part 1 1.2). Specifically, for samples crystallized at low crystallization temperatures (T_c) , 1.00 \pm 0.05 mg of polymer was first dissolved in a measured amount of chloroform at the desired T_c . This step was followed by mixing the PHBHx chloroform solution with a measured amount of ethanol (total amount of chloroform and ethanol was kept at 10 g) at T_c to form a supercooled polymer solution, which was then allowed to crystallize for 21 h. For samples crystallized at a high T_c , $1.00 \pm 0.05 \,\mathrm{mg}$ of polymer was first dissolved in a 10 g mixture of chloroform and ethanol at the desired molar ratio at a dissolution temperature of 110 °C for 30 min. The resulting solution was quenched to a desired T_c and allowed to fully crystallize for 21 h. The concentration of all the samples was kept at 0.01 wt%. For XRD, FTIR, and DSC measurements, single crystal suspensions were hot filtered, followed by drying under vacuum overnight to remove residual solvent.

3. Characterization

3.1. Transmission electron microscopy (TEM)

A Tecnai G²-12 TEM operating at 120 kV was used to investigate the morphology and crystal structure of PHBHx single crystals. Droplets of crystal suspensions were deposited on a 300-mesh copper-grid substrate with an ultra-thin coated carbon film. The camera length used for recording the electron diffraction pattern was 2.1 m. A polycrystalline aluminum standard sample with a cubic lattice of $a=0.4041\,\mathrm{nm}$ (determined by XRD) was used for calculating the unit cell parameters of PHBHx crystals.

3.2. Determination of critical electron dose

The critical radiation dose measures the ability of an organic crystalline material to resist the electron beam damage [20]. Experiments evaluating the critical electron dose for PHBHx single crystals were carried out using the (110) reflection for the measurement. Details on the measurement method can be found in supporting information part 3. The equation below was used to extract the critical dose [21]

$$I(D) = I_0 exp\left(-\frac{D}{D^*}\right) + I_R$$

where I_0 is the initial diffraction intensity before the reflection begins to decay due to the electron beam damage, I_R is the residual intensity

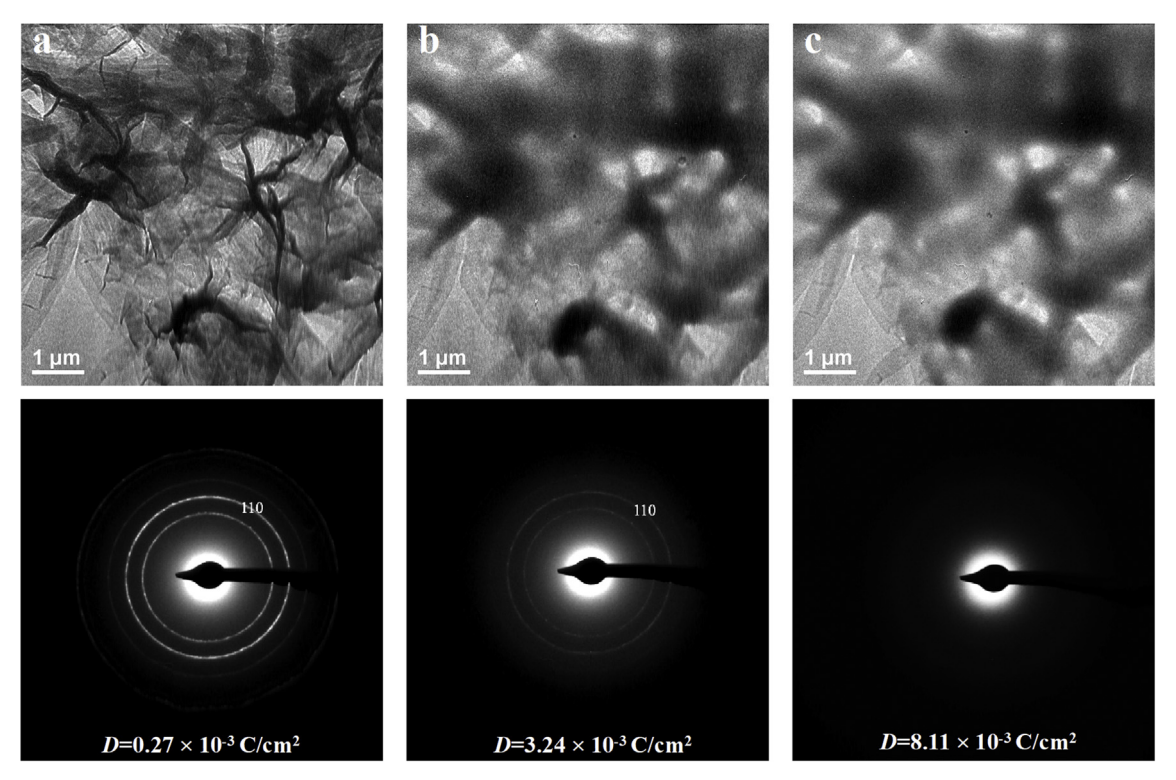


Fig. 1. Bright field TEM morphology image (top) and electron diffraction patterns (bottom) of PHBHx crystal aggregates at different doses. 0.27×10^{-3} C/cm² (A), 3.24×10^{-3} C/cm² (B), and 8.11×10^{-3} C/cm² (C).

including background and scattering from the damaged sample, and D^{\star} is the critical dose, which is the reciprocal of exponential decay constant. Therefore, a higher value of D^{\star} indicates a slower diffraction intensity decay. For simplicity, we directly report the measured critical dose of PHBHx single crystals in this experimental section.

Fig. 1 shows the variation of crystal morphology and corresponding electron diffraction patterns (EDPs) with increasing electron doses of 0.27×10^{-3} , 3.24×10^{-3} and 8.11×10^{-3} C/cm², respectively. We can see from Fig. 1a-c that the initial crystal structure with well-defined contours transforms to a featureless, rounded structure. However, no obvious morphological change such as material flowing, or mass loss can be identified, but the diffraction intensity is dramatically reduced. This result suggests that PHBHx single crystal experienced a crosslinking process during high energy electron radiation. Electron radiation induced crosslinking has been reported for polymers such as PE, and was presumed to arise from radicals generated during exposure [22]. The critical dose D^* was determined derived by fitting a linear plot of the logarithm of integrated area of diffraction intensity of (110) reflection against electron dose (details see supporting information part 3). The D^* was obtained for all the different T_c grown crystals. We found that PHBHx (3.9 mol%) single crystals have a D* on the order of 10⁻² C/cm², which is a little higher than that of PE single crystals at similar operation voltages (0.0043 at 100 kV and 0.012 at 125 kV), and similar to Nylon-6 crystals [18,23].

3.3. X-ray diffraction

A Bruker D8 diffractometer was operated at 40 kV and 40 mA with an X-ray wavelength of 1.5418 Å (Cu K α radiation). One-dimensional, XRD experiments in reflection geometry (theta-theta) mode were conducted by positioning a crystal mat flat on the sample stage. Diffraction profiles were recorded by scanning 20 from 10 to 40° with a 0.05° resolution and a 0.5 s exposure time per step.

3.4. Fourier transform infrared spectroscopy

Infrared experiments were conducted using a Thermo Nicolet 670 Nexus FT-IR spectrometer with a DTGS detector operating in attenuated total reflection (ATR) mode using a Specac Golden Gate ATR accessory. The spectra were obtained by averaging 128 scans from $600\,{\rm cm}^{-1}$ to $4000\,{\rm cm}^{-1}$ with a resolution of $2\,{\rm cm}^{-1}$. The raw spectra were then processed using the Essential FTIR software for baseline correction and advanced ATR correction.

4. Results and discussion

4.1. Temperature-dependent anisotropic lateral growth habit

During non-self-seeded isothermal crystallization, a nucleation barrier needs to be overcome, which typically gives rise to a small number of nuclei. Giant, poorly-defined spherulites (due to low concentration) will then develop with lamellae spreading out radially. Thus, single-layered lamellae can typically be found on the edges of these spherulites. Also, these crystals are developed well after the solution reaches the desired crystallization temperature so that the isothermal crystallization process is more rigorous. Micrographs of crystal morphologies and electron diffraction patterns were all recorded on these single-layered crystals to reflect the intrinsic crystal property. Surprisingly, for experiments conducted for all the T_c (except for T_c -20 °C), PHBHx was able to form single crystals with well-defined crystal geometry. This observation is very intriguing since it is generally accepted that a random copolymer with such a high defect content cannot form well-defined single crystals. Indeed, for PE, with only 1.13 mol% of 1-pentene statistically distributed on the backbone, the resultant crystals grown from dilute solution had irregular shapes, and deviated from the well-known lozenge shape of typical PE single crystals. In addition, we found out that 3HHx was not included in the lattice at normal temperatures (except for the case of T_c -20 °C) as determined by the lattice parameter measurements. This situation is also

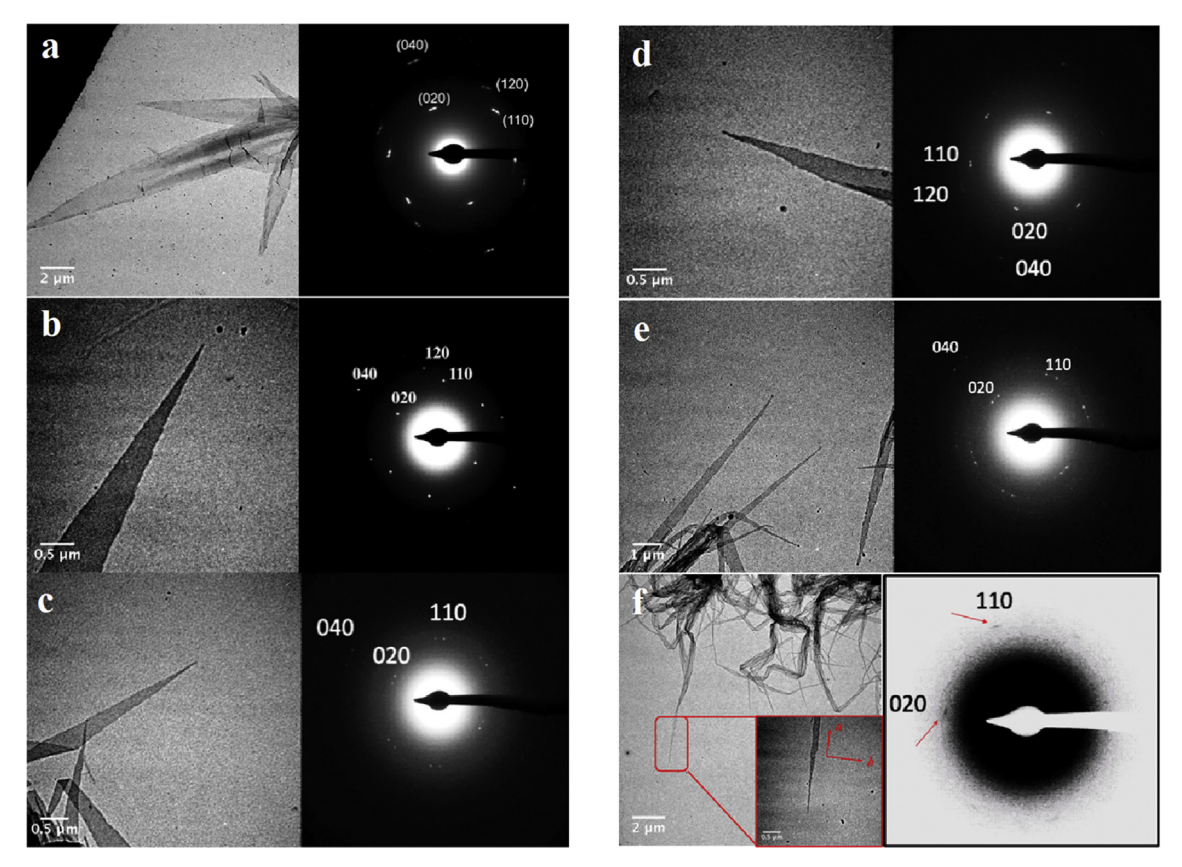


Fig. 2. Figure a to f show micrographs and corresponding electron diffraction patterns of single crystals crystallized at 75, 65, 60, 55, 40, and 20 °C, respectively. Diffraction pattern in f corresponds to the needle-shaped crystal in the inset. Due to its narrow nature, the diffraction intensity is low even after increasing the graph contrast manually. To guide the eye, the two reflections (020) and (110) are indicated with red arrows. (For interpretation of the references to color in this figure legend, the reader is referred to the Web version of this article.)

different from propyl-branched PE for which an incorporation of 3.1 mol% of pentene results in an a-lattice expansion from 0.742 nm to 0.747 nm [24].

The morphology and electron diffraction pattern (EDP) of PHBHx single crystals as a function of crystallization temperature are shown in Fig. 2 starting from $T_{\rm c}=75\,^{\circ}{\rm C}$ (Fig. 2a). The crystals show a needle-like structure, similar to solution grown single crystals of the homopolymer, PHB [25,26]. The EDP can be indexed with the [001] zone of the α form of homopolymer, PHB. Measured lattice parameters of a and b have values 0.574 nm, and 1.324 nm \pm 0.003 nm, respectively. These values agree well with those found for PHB thin film using XRD and those for PHBHx bulk samples [9,27], suggesting that 3HHx was not included within the unit cells. In addition, coupled with diffraction indexing, we can identify that the growth direction is along the a-axis of the unit cell. The highly elongated needle-shaped crystal further indicates that the growth rate of the crystal along the a axis is faster than that along the b-axis.

Following the order of decreasing crystallization temperatures, morphologies and EDPs for single crystals crystallized at 65, 60, 55, 40, and 20 °C are shown in Fig. 2b–f, respectively. Though the indexing of EDPs, d-spacing and diffraction symmetry for all these samples are the same as those for the case of $T_{\rm c}=75$ °C, the reflection intensities are much weaker. This was due to the fact that the crystals tend to become narrower with decreasing $T_{\rm c}$ so that the amount of material contributing to the diffraction intensity is also reduced. This phenomenon can most clearly be seen in the $T_{\rm c}=20$ °C crystals (Fig. 2f). The crystal is highly anisotropic, with a width of only around 10 nm, which can be seen from the magnified crystal section in Fig. 2f inset. Recording electron diffraction patterns for this crystal was very difficult due to the narrow nature of the single crystal. With inverted color, however, very

dim diffraction spots can be identified.

The variation in the apparent apex angle as a function of T_c suggests that the relative growth rates of the crystal along the a and b axes have different thermal dependences. By measuring the apex angle, we can semi-quantitatively determine the growth rates of the crystal along two directions. The growth rate (length time $^{-1}$) ratio can be derived from tan(theta/2) (theta is the apex angle). Given the fact that the unit cell is highly anisotropic, i.e., b is over two times longer than a (b/a = 2.3), it would be insightful to compare the two apparent growth rates divided by each lattice constant. By doing this, we are effectively comparing unit cell packing rate along the two directions (number of unit cell time⁻¹). For each sample, the value of the apex angle was obtained by averaging the measured angles of 36 different crystals (detailed statistics for each sample see supporting information part 2). A plot of measured apex angle, growth rate ratio, and unit cell packing rate along the a and b axes as a function of T_c is shown in Fig. 3. We can clearly see from the plot that, at $T_c = 75$ °C, the growth rate along the a-axis was about 7 times faster than that along the b-axis, whereas at $T_c = 20$ °C, this ratio increased to 24. As for unit cell packing rate, at $T_c = 20$ °C, the packing velocity along the a-axis was nearly 55 times faster than that along the b-axis. Such significant packing rate difference surely will result in the formation of the sharp needle-shaped single crystal.

In a conventional sense, the significantly faster unit cell packing rate along the *a*-axis indicates that along this direction certain strong molecular interactions between packing stems would exist, such as –OH··O or –NH··O hydrogen-bonding. However, PHBHx is a polyester without any high binding-energy interactive groups. Therefore, it is worth investigating the specific molecular packing fashion involved in the PHBHx single crystal unit cell. The crystal structure was rebuilt using coordinates reported by Wang and Tashiro, as shown in Fig. 4. We use

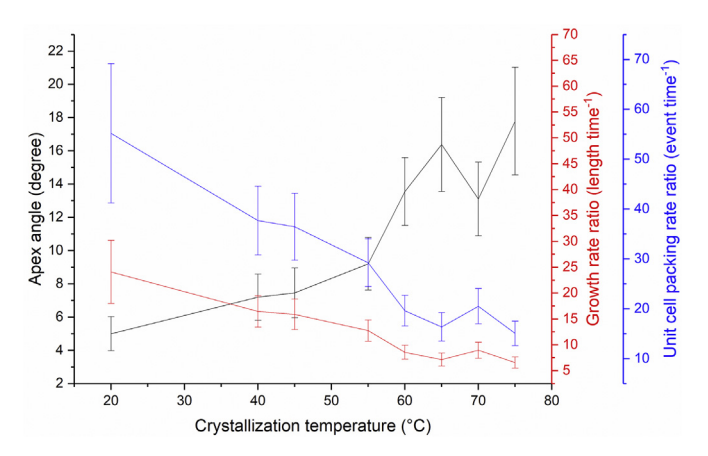


Fig. 3. Plot of crystal apex angle, growth rate ratio, and unit cell packing rate ratio along the *a*- and *b*-axes as a function of crystallization temperatures. Each data point is the averaged apex angle value based on 36 measured crystals. Error bar represents the standard deviation within 36 measurements. (Measurement details and histograms see supporting information part 2).

blue and green dashed lines to highlight the weak H-bonding formed between one of the methyl hydrogens and the carbonyl oxygen. Fig. 4A is the c-projection, where one can clearly see that, along the a-axis, the stems are connected by a network of hydrogen bonds, whereas along the b-axis, the inter-stem interaction is dominated by Van der Waals interactions. Several more intriguing features can be seen by examining the crystal packing style along b, as shown in Fig. 4B. Taking the middle stem in Fig. 4B as an example, one can make several observations. First, within the unit cell (black square), there are two repeating 3HB units; the lower repeating unit forms two hydrogen bonds with its right neighboring stem, whereas the upper repeating unit forms two hydrogen bonds with its left neighboring stem. Second, the methyl carbon and carbonyl oxygen from the same 3HB unit are almost at the same z height in the unit cell, but the two H-bonds that the two atoms engage to form point towards opposite directions (blue-colored H-bond towards up and green-colored one towards down). Therefore, such a packing pattern results in a dense H-bond propagation along the *c*-axis, and each of the stems is stabilized by its neighboring stems along the adirection through the formation of four anchoring H-bonds. Thus, despite a relatively low binding energy of -C-H-O, less than 4 kJ mol⁻¹ as estimated by Sato et al. [8], the appearance of such a highly dense cooperative H-bonding framework and the directionality of the H-bonds

results in a much higher stem packing rate along the a-axis. It is worth noting that such an elongated needle shape has also been observed in polyamides, such as Nylon 6,10 and poly(hexamethylene terephthalate) crystals formed from dilute solution [28]. However, these polymers are believed to have their molecular chains nearly parallel to the crystal long axis, as opposed to PHBHx crystals crystallized at low $T_{\rm c}$, which have their molecular chains oriented perpendicular to the lamellar surface through chain-folding.

Thermally dependent anisotropic growth habits can also be seen in XRD data (Fig. 5) on single crystal mats. The crystallite domain size was evaluated using the Scherrer equation. The crystallite size along the b direction increases from 13.8 nm to 27.4 nm, from $T_{\rm c}=20\,^{\circ}{\rm C}-75\,^{\circ}{\rm C}$ (Fig. 5B). Though the crystallite dimension along the a direction is hard to obtain using the (110) peak due to the overlap with (011), the significant increase in the dimension along the b direction is still an indication that at higher $T_{\rm c}$, the anisotropic growth habit is attenuated, which is consistent with TEM observations.

4.2. Lamellar thickness

The crystallite dimension along the chain axis (lamellar thickness) was evaluated using the (002) peak as shown in Fig. 5B. Noticeably, the lamellar thickness found for crystals grown at $T_c = 75$ °C in our case is smaller than that seen for bulk crystallized homopolymer PHB [29]. Without 3HHx defects, single crystals produced from a solution should possess a thicker lamella due to a higher nucleation energy barrier arising from the existence of significant amounts of a good solvent (chloroform). This result suggests that in some way the 3HHx prevents the thickening of PHBHx lamellae. Actually, the theoretical maximum lamellar thickness calculated using a simple mean field model shows this is indeed the case. For PHBHx (3.9 mol%), when the possibility of consecutively adding 3HB to a stem reaches 50%, the required number of 3HB units can be obtained as $log_{(1-3.9\%)}0$. 5 = 17.42, corresponding to an \sim 5.19 nm lamellar thickness. The result indicates that the typical lamellae cannot be thicker than this number. Thus, we can see that at $T_c = 75$ °C, the measured thickness 4.54 nm is close to this threshold with around one repeat unit difference (recall parameter c = 0.596 nm). It then suggests that even at 75 °C, the crystalline motif of 3HB is not fully utilized. Possibly this result is due to the 3HB units in the vicinity of 3HHx not being able to enter into the lattice due to a high folding energy involved in the folding process. More importantly, it suggests that the critical stable nuclei size required for crystallization of PHBHx is not required to be large, manifesting the superior stability of

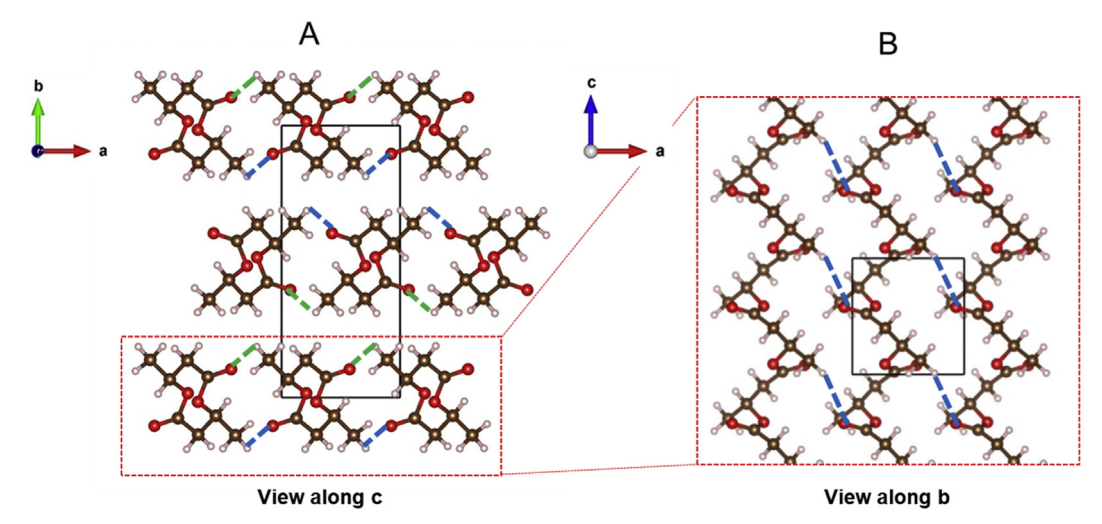


Fig. 4. Projection along the *c*-axis (A) and *b*-axis (B) of unit cell structure of PHB. Unit cell structure is rebuilt using atomic coordinated determined by Wang and Tashiro [9]. The b-projected picture (B) is from the layer highlighted with red dash square in A. (For interpretation of the references to color in this figure legend, the reader is referred to the Web version of this article.)

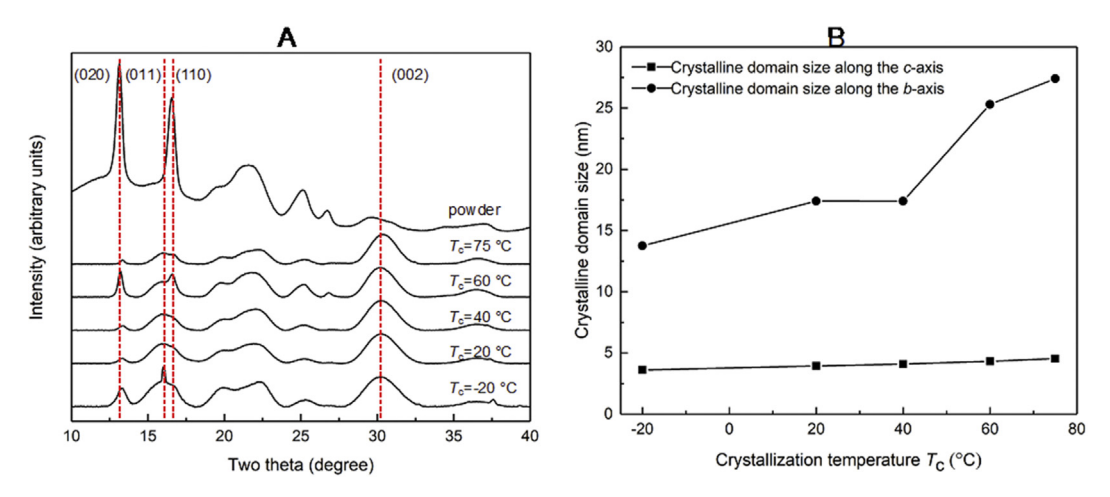


Fig. 5. A: 1-D XRD pattern of a PHBHx single crystal mat at different crystallization temperatures. For comparison, the powder diffraction pattern is also attached. B: Plot of crystallites size derived from the (020) and the (020) peak from A as a function of crystallization temperature.

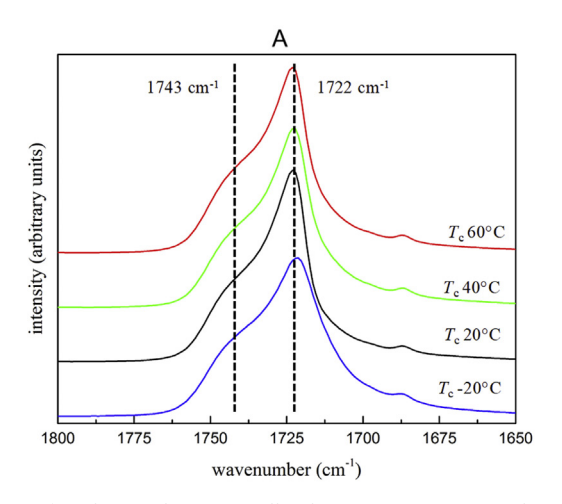
the PHBHx crystal lattice. The lamellar thickness for single crystals crystallized at $T_{\rm c}=-20\,^{\circ}{\rm C}$ is even thinner with an unusually small value of 3.6 nm, which corresponds to only 6 3HB repeating units. In this case, a larger number of 3HB units are excluded at the fold surface as disordered amorphous material. This finding regarding the ultra-thin lamellae could provide another insight for the difficulty of inhibiting PHB crystallization. That is, to form a stable nucleus, the polymer only needs a relative small amount of consecutively connected 3HB repeating units. In the single crystal regime, it acts in a way that the random copolymer is still able to form a well-developed single crystal by forcing the 3HHx into the amorphous region.

The above analysis can also be supported by infrared spectroscopy (Fig. 6), which is sensitive to variation in the local environment of various chemical functional groups, providing valuable information regarding the fold surface. From the carbonyl region (Fig. 6A), it is seen that even at high $T_{\rm c}=75\,^{\circ}{\rm C}$, there are still significant amounts of amorphous material, indicated by the band 1743 cm $^{-1}$ associated with the amorphous component [30]. These disordered chain segments are from the non-crystalline PHBHx in the vicinity of those 3HHx units. Noticeably, for the –CH stretching region (Fig. 6B), we can clearly identify the H-bonding signature shoulder, located at 3009 cm $^{-1}$, especially for high $T_{\rm c}$ grown crystals. However, one can see as $T_{\rm c}$ decreases, there is a decreased lamellar thickness, and the shoulder becomes less obvious. Especially, when reaching $T_{\rm c}=-20\,^{\circ}{\rm C}$, the 3009 cm $^{-1}$ peak is buried in the broad –CH stretching band. This observation indicates that a larger number of free-state 3HB was located

in the fold surface (not restricted by H-bonding network). Indeed, due to a decreased chain mobility at low $T_{\rm c}$, more crystalline units of 3HB in the vicinity of 3HHx could not actually crystallize but instead are excluded on the fold surface.

4.3. The effect of 3HHx manifested at low temperature $-20^{\circ}C$

The effect of incorporation of 3HHx defects on crystal growth habits starts to be visible at a very low crystallization temperature, -20 °C, as shown in the TEM morphological graph and EDP in Fig. 7. No more well-developed, surface-smooth, shape-regular crystals can be identified. Instead, one can identify a twisted lamellar structure, as highlighted in Fig. 7A. Although the driving force for the mechanism of lamellar twisting has been debated [31,32], the twisting in our case is most likely occurring to allow the cumulative stress to be released due to an overcrowded fold surface. The twisted lamellar structure can also be seen by XRD in Fig. 5A. In the $T_c = -20$ °C trace, the (011) diffraction peak is much more intense than that for crystals crystallized at higher T_c . This result suggests that a significant amount of the lamellar crystals twisted around the a-axis (the growth direction) leading to the detection of (011) planes by the 1-D XRD. If there was no twisting or the frequency of twisting was low, most of the crystals would lie flat on the substrate (due to filtration process), leading to a higher (002) peak in the trace, as seen for higher T_c crystals. The preferred orientation of single crystal mats can also be seen by comparing with a randomly oriented powder sample, in which the relative intensity of (002) peak is



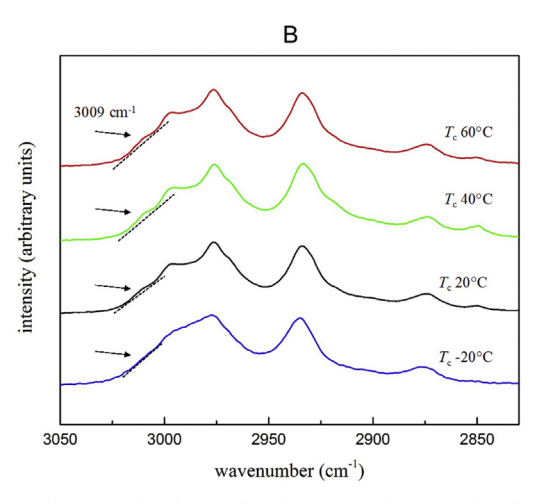


Fig. 6. FTIR spectra of single crystal mats crystallized at $T_c = -20$, 20, 40 and 60 °C. A: absorption band for carbonyl region. B: absorption band for –C–H stretching region.

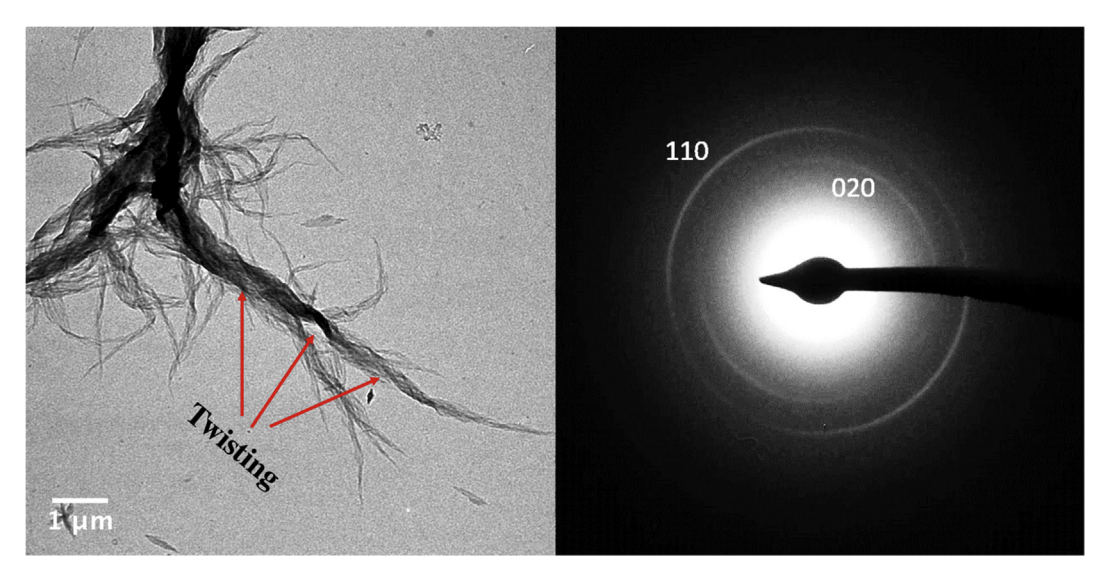


Fig. 7. The morphology of twisted single crystals and diffraction pattern of T_c – 20 °C crystallized crystals.

very low.

Interestingly, also at this crystallization temperature, the b parameter expanded to 1.330 nm \pm 0.003 nm from 1.324 nm for crystals grown at higher $T_{\rm c}$. Based on this diffraction result, we didn't observe such a significant change in the a direction indicated by the fact that a=0.573 nm at $T_{\rm c}=-20\,^{\circ}{\rm C}$ whereas, a=0.574 nm at higher temperatures. Though accommodation of 3HHx defects along the a axis could still occur, it is clear that accommodation of 3HHx comonomer units along the b direction has a higher probability. Because H-bonding is along the a direction, including too many defects would significantly decrease crystal stability, whereas due to a relatively weaker intermolecular interaction along the b-direction, it would result in a higher probability for the defects to be accommodated along this direction.

4.4. A comparison between PHBHx and poly[(R)-3-hydroxybutyrate-co-(R)-3-hydroxyvalerate] (PHBV)

To this point, it is of interest to further compare the mechanism of the role of 3HHx units in affecting the crystallization of PHBHx to that of 3HV affecting the crystallization of PHBV. Due to the fact of isodimorphic cocrystallization, the crystallinity of PHBV was not disrupted significantly. However, the enthalpy of fusion was definitely decreased, which can be seen from the melting point depression down to $\sim 80\,^{\circ}\text{C}$ (3HV content 29 mol%) [16,33]. It, therefore, implies that, for bulk state, it is expected that the number of inter-crystalline amorphous chains would not be increased significantly compared with that of PHB, and the cohesive energy of crystalline domain was observed to decrease. This implies that the ultimate toughness of PHBV would not be substantially improved compared with that of PHB [1,2]. However, for PHBHx, the crystallinity can be reduced by excluding 3HHx and 3HB units in the vicinity of 3HHx from the lattice. This exclusion results in thinner lamellae, which gives rise to a lower melting point. However, it should be noted that the mechanism of the melting point depression between PHBHx and PHBV may be fundamentally different. The former is due to decreased lamellar thickness whereas the latter is due to lowered cohesive energy of the crystals. Though the lamellae are ultrathin, the crystal structure is still stable due to the compact hydrogen bonding network. Therefore, it should be expected that PHBHx would have an improved toughness compared with PHB. Another difference between PHBHx and PHBV can be seen from the specific way 3HHx and 3HV are incorporated in the crystal lattice. As indicated previously, the 3HHx can be included into the lattice only at a very low temperature of $T_c = -20$ °C. However, for PHBV, it is reported that the inclusion of 3HV comonomer in the crystal structure can occur over a wide range of temperatures, and the inclusion is always along the a direction due to cocrystallization of two components of 3HB and 3HV [16]. This difference was believed due to the fact that when crystallizing, PHV and PHB share a similar chain conformation in their crystal structures.

5. Conclusions

In the present study, we have investigated crystallization habits of bacterially produced copolyester PHBHx in dilute solutions. We were able to grow single crystals of PHBHx (3.9 mol%) from a chloroform/ethanol mixture at different crystallization temperatures ranging from $-20\,^{\circ}\mathrm{C}$ to 75 $^{\circ}\mathrm{C}$. Crystal structures and morphologies of all the crystals were investigated by electron diffraction, X-ray diffraction, and FTIR. The following conclusions can be draw from this study:

- 1. PHBHx at a moderately high 3HHx content still remains remarkably crystallizable. This is manifested by the fact that across a wide range of crystallization temperatures, PHBHx was able to form well-developed, laterally smooth lamella, which is in contrast to typical random copolymers. PHBHx single crystals exhibit very thin lamellae with thicknesses down to 3.6 nm, indicating superior crystal structure stability. We conclude that PHBHx crystallization is attributed to a cooperative H-bonding network that forms to stabilize its crystal structure. Though the bonding energy is relatively weak (< 4 kJ/mol), the packing density is high, leading to an equivalent stabilization effect. In addition, the observed highly thermal dependent anisotropic growth habit of PHBHx single crystals is also a manifestation of the existence of weak H-bonding network, indicated by the fact that the faster growth direction of the crystal is parallel with H-bonding direction.</p>
- 2. For all crystallization temperatures, the 3HHx comonomer serves to decrease lamellar thickness, resulting in a thinner crystal compared with that of PHB crystallized at the same temperature. In addition, a more significant influence of 3HHx on crystallization habits of PHBHx begins to be observed at quite a low crystallization temperature $T_{\rm c} = -20\,^{\circ}\text{C}$. At this temperature, due to a lower chain flexibility, 3HHx was incorporated kinetically between (020) planes. To further disrupt the crystal structure to improve the materials mechanical properties at normal temperatures, a higher content of 3HHx would be required,

Acknowledgements

The authors would like to acknowledge the support from Delaware

NSF EPSCoR Grant # 1301765 and the NSF DMR Polymers Program Grant DMR-1407255. DCM thanks the NSF through Polymers Program Grant DMR-1103027.

Appendix A. Supplementary data

Supplementary data related to this article can be found at https://doi.org/10.1016/j.polymer.2018.08.046.

References

- I. Noda, P.R. Green, M.M. Satkowski, L.A. Schechtman, Preparation and properties of a novel class of polyhydroxyalkanoate copolymers, Biomacromolecules 6 (2) (2005) 580–586.
- [2] I. Noda, S.B. Lindsey, D. Caraway, Nodax™ class PHA copolymers: their properties and applications, in: G.G.-Q. Chen (Ed.), Plastics from Bacteria, vol. 14, Microbiology Monographs; Springer, Berlin, 2010, pp. 237–255.
- [3] Stephen Philip, Tajalli Keshavarz, Ipsita Roy, Polyhydroxyalkanoates: biodegradable polymers with a range of applications, J. Chem. Technol. Biotechnol. 82 (3) (2007) 233–247.
- [4] Bronwyn Laycock, et al., The chemomechanical properties of microbial polyhydroxyalkanoates, Prog. Polym. Sci. 38 (2013) 3-4 536-583.
- [5] Adchara Padermshoke, et al., Thermally induced phase transition of poly (3-hy-droxybutyrate-co-3-hydroxyhexanoate) investigated by two-dimensional infrared correlation spectroscopy, Vib. Spectrosc. 36 (2) (2004) 241–249.
- [6] Jenny Josefine Fischer, et al., Mechanical properties and enzymatic degradation of poly ([R]-3-hydroxybutyrate-co-[R]-3-hydroxyhexanoate) uniaxially cold-drawn films, Polym. Degrad. Stabil. 83 (3) (2004) 453–460.
- [7] Hideki Abe, et al., Solid-state structures and enzymatic degradabilities for meltcrystallized films of copolymers of (R)-3-hydroxybutyric acid with different hydroxyalkanoic acids, Macromolecules 31 (6) (1998) 1791–1797.
- [8] Harumi Sato, et al., Infrared spectroscopy studies of CH-O hydrogen bondings and thermal behavior of biodegradable poly (hydroxyalkanoate), Macromolecules 37 (19) (2004) 7203–7213.
- [9] Hai Wang, Kohji Tashiro, Reinvestigation of crystal structure and intermolecular interactions of biodegradable poly (3-hydroxybutyrate) α-form and the prediction of its mechanical property, Macromolecules 49 (2) (2016) 581–594.
- [10] Maryon W. Dougill, G.A. Jeffrey, The structure of dimethyl oxalate, Acta Crystallogr. 6 (1953) 11–12 831-837.
- [11] Gautam R. Desiraju, Thomas Steiner, The Weak Hydrogen Bond: in Structural Chemistry and Biology vol. 9, International Union of Crystal, 2001.
- [12] Hiroatsu Matsuura, et al., Experimental evidence for intramolecular blue-shifting C − H⊙⊙⊙ O hydrogen bonding by matrix-isolation infrared spectroscopy, J. Am. Chem. Soc. 125 (46) (2003) 13910–13911.
- [13] Rabi A. Musah, et al., Variation in strength of an unconventional C H to O hydrogen bond in an engineered protein cavity, J. Am. Chem. Soc. 119 (38) (1997) 9083–9084.
- [14] Senes, Alessandro, Iban Ubarretxena-Belandia, and Donald M. Engelman. The Cα—H··· O hydrogen bond: a determinant of stability and specificity in transmembrane helix interactions. Proc. Natl. Acad. Sci. Unit. States Am. 98.16 (200).
- [15] P.J. Barham, et al., Crystallization and morphology of a bacterial thermoplastic:

- poly-3-hydroxybutyrate, J. Mater. Sci. 19 (9) (1984) 2781-2794.
- [16] Terry L. Bluhm, et al., Isodimorphism in bacterial poly (β-hydroxybutyrate-co-β-hydroxyvalerate), Macromolecules 19 (11) (1986) 2871–2876.
- [17] Toru Kawai, Közaburo Ujihara, H. Maeda, Fold structure of solution grown crystals of alkyl-branched copolymers of polyethylene, Macromol. Chem. Phys. 132 (1) (1970) 87–111.
- [18] G. Adamus, W. Sikorska, M. Kowalczuk, I. Noda, M.M. Satkowski, Electrospray ion-trap multistage mass spectrometry for characterisation of co-monomer compositional distribution of bacterial poly (3-hydroxybutyrate-co-3-hydroxyhexanoate) at the molecular level, Rapid Commun. Mass Spectrom. 17 (20) (2003) 2260–2266.
- [19] R.H. Marchessault, S. Coulombe, H. Morikawa, K. Okamura, J.F. Revol, Solid state properties of poly-β-hydroxybutyrate and of its oligomers, Can. J. Chem. 59 (1) (1981) 38–44.
- [20] L.F. Drummy, J. Yang, D.C. Martin, Low-voltage electron microscopy of polymer and organic molecular thin films, Ultramicroscopy 99 (4) (2004) 247–256.
- [21] S. Kumar, W.W. Adams, Electron beam damage in high temperature polymers, Polymer 31 (1) (1990) 15–19.
- [22] D.T. Grubb, G.W. Groves, Rate of damage of polymer crystals in the electron microscope: dependence on temperature and beam voltage, Philos. Mag. A 24 (190) (1971) 815–828.
- [23] H. Sato, M. Nakamura, A. Padermshoke, H. Yamaguchi, H. Terauchi, S. Ekgasit, I. Noda, Y. Ozaki, Thermal behavior and molecular interaction of poly (3-hydroxybutyrate-co-3-hydroxyhexanoate) studied by wide-angle X-ray diffraction, Macromolecules 37 (10) (2004) 3763–3769.
- [24] Paul R. Swan, Polyethylene unit cell variations with branching, J. Polym. Sci. Polym. Chem. 56 (164) (1962) 409–416.
- [25] Tadahisa Iwata, et al., Alkaline hydrolysis of solution-grown poly [(R)-3-hydro-xybutyrate] single crystals, Macromolecules 32 (25) (1999) 8325–8330.
- [26] Tadahisa Iwata, et al., Visualization of enzymatic degradation of poly [(R)-3-hy-droxybutyrate] single crystals by an extracellular PHB depolymerase, Macromolecules 30 (4) (1997) 833–839.
- [27] M. Yokouchi, et al., Structural studies of polyesters: 5. Molecular and crystal structures of optically active and racemic poly (β-hydroxybutyrate), Polymer 14 (6) (1973) 267–272.
- [28] A. Keller, R. Engleman, Electron microscope-electron diffraction investigations of the crystalline texture of polyamides, J. Polym. Sci., Part A: Polym. Chem. 36 (130) (1959) 361–387.
- [29] Hideki Abe, et al., Solid-state structures and enzymatic degradabilities for meltcrystallized films of copolymers of (R)-3-hydroxybutyric acid with different hydroxyalkanoic acids, Macromolecules 31 (6) (1998) 1791–1797.
- [30] I. Noda, A.E. Dowrey, J.L. Haynes, C. Marcott, Group frequency assignments for major infrared bands observed in common synthetic polymers, in: J.E. Mark (Ed.), Physical Properties of Polymers Handbook, Springer, New York, NY, 2007, pp. 395–406.
- [31] Jun Xu, et al., Direct AFM observation of crystal twisting and organization in banded spherulites of chiral poly (3-hydroxybutyrate-co-3-hydroxyhexanoate), Macromolecules 37 (11) (2004) 4118–4123.
- [32] H.D. Keith, W.Y. Chen, On the origins of giant screw dislocations in polymer lamellae, Polymer 43 (23) (2002) 6263–6272.
- [33] Masao Kunioka, Akira Tamaki, Yoshiharu Doi, Crystalline and thermal properties of bacterial copolyesters: poly (3-hydroxybutyrate-co-3-hydroxyvalerate) and poly (3hydroxybutyrate-co-4-hydroxybutyrate), Macromolecules 22 (2) (1989) 694–697.